Water Research 111 (2017) 140–146

Contents lists available at ScienceDirect

Water Research

journal homepage: www.elsevier.com/locate/watres

Potential effects of loading nano zero valent iron discharged on membrane fouling in an anoxic/oxic membrane bioreactor

Lijie Zhou [a, b], Weiqin Zhuang [c], Xin Wang [b], Ke Yu [d], Shufang Yang [e], Siqing Xia [b, *]

[a] State Environmental Protection Key Laboratory of Drinking Water Source Management and Technology, Shenzhen Key Laboratory of Drinking Water Source Safety Control, Shenzhen Key Laboratory of Emerging Contaminants Detection & Control in Water Environment, Shenzhen Academy of Environmental Sciences, Guangdong Shenzhen 518001, China
[b] State Key Laboratory of Pollution Control and Resource Reuse, College of Environmental Science and Engineering, Tongji University, 1239 Siping Road, Shanghai 200092, China
[c] Department of Civil and Environmental Engineering, University of Auckland, Auckland 1142, New Zealand
[d] School of Environment and Energy, Peking University Shenzhen Graduate School, Guangdong Shenzhen 518055, China
[e] Shenzhen Municipal Design & Research Institute Co., Ltd, 3007 West Sungang Road, Guangdong Shenzhen 518029, China

ARTICLE INFO

Article history:
Received 21 August 2016
Received in revised form
8 December 2016
Accepted 2 January 2017
Available online 3 January 2017

Keywords:
Nano zero valent iron (nZVI)
Membrane bioreactor
Membrane fouling
Reactive oxygen species

ABSTRACT

A laboratory-scale submerged anoxic-oxic membrane bioreactor for municipal wastewater was operated to investigate the potential effects of loading suspended nano zero valent iron (nZVI, 25 and 50 mg/L) discharged on the membrane fouling. nZVI transformed rapidly into Fe^{n+}, generated reactive oxygen species (ROS) and caused oxidative stress. This result rapidly led to the cell lysis and bacteria death, and further resulted in the decrease of biomass and extracellular polymeric substances (EPS). nZVI also thinned the membrane fouling layer. But nZVI had no obvious effects on activated sludge particle size, EPS molecule weight distribution and VOCs constitution of membrane foulant. Additionally, nZVI released Fe^{n+} and mitigated the inorganic (mainly Si element) fouling through Fe^{n+} flocculation. Consequently, membrane fouling mitigation with nZVI discharged was mainly due to oxidative stress to bacteria and Fe^{n+} flocculation of nZVI.

1. Introduction

Nanoparticles (NPs), which are particulate matter with at least one dimension lower than 100 nm, play an increasingly important role in medical device and diagnostics, construction, electronics and environmental remediation (Bagheri and Julkapli, 2016; Feng et al., 2016). Among NPs, nano zero valent iron (nZVI) is considered as the new environmental remediation technology, which is the cost-effective solution to some of the most challenging environmental clean-up problems. nZVI is currently applied for the soil and groundwater remediation based on two chemistry pathway: (1) nZVI acts as an electron donor to break down or to convert contaminant into a less toxic or mobile form; (2) nZVI works as a sorbent-, (co)precipitant- or contaminant-immobilising agent (Lefevre et al., 2016; Sacca et al., 2013). nZVI is also promising for the removal of pharmaceuticals, halogenated organic compounds, pesticides, viruses, etc. in the future (Sevcu et al., 2012).

However, the unique catalytic properties of nZVI have led to concerns regarding their potential harmful impacts on indigenous organisms in environment (Lefevre et al., 2016; Patil et al., 2016). Although nZVI treatment is a well acceptable practice in United State, few applications have been carried out in Europe, due to the potential health risks (Sacca et al., 2014). nZVI is toxic to pure-cultured bacteria in concentrations as low as a few mg/L (Otero-Gonzalez et al., 2013; Sacca et al., 2013; Sevcu et al., 2012). The attachment of NPs to the bacterial surface leads to the decrease of both cell mobility and nutrient between the cell exterior and interior compartments (Navarro et al., 2008). In addition, nZVI can cause rapid generation of free radicals. Fe^{2+}, as the outcome of redox-active nZVI reacts, can generate reactive oxygen species (ROS) with free radicals (Fenton or Fenton-like reaction) (Sevcu et al., 2012). Elevated concentrations of ROS in a cell results in the oxidative stress, which causes various dysfunctions of membrane lipids, proteins and DNA, etc., and further ends in apoptosis or death of the microorganisms (Davies, 2000). nZVI aggregates rapidly into micrometer or even larger particles in environment

* Corresponding author.
E-mail address: siqingxia@gmail.com (S. Xia).

http://dx.doi.org/10.1016/j.watres.2017.01.007
0043-1354/

due to the nano-size adsorption (Lefevre et al., 2016), indicating that nZVI keeps hardly in the form of nano-size. Therefore, compared with long-term effects of nZVI, the potential risk of loading nZVI discharged into environment should be concerned.

This study aimed to investigate the potential effects of loading nZVI discharged on the performance and membrane fouling in an anoxic/oxic membrane bioreactor (MBR) for municipal wastewater. The performance, activated sludge characteristics and membrane fouling were measured with various methods, including gas chromatography-mass spectrometry (GC-MS), scanning electron microscopy (SEM), line-analysis of energy-dispersive X-ray (EDX), etc.

2. Methods and materials

2.1. Preparation of nZVI suspension

nZVI (>99.9%, approximate 50 nm) was purchased from Aladdin (Shanghai, China) in this study. 500 mg nZVI was sonically distributed (25 °C, 300 W, 40 kHz) in 1 L anaerobic MilliQ-water for 2 h to prepare stock nZVI suspension (500 mg/L) according to Zhou et al., (2014c). The primary size of nZVI in stock suspension was in the range of 50–100 nm (Fig. 1), which was close to the particle size provided by Aladdin.

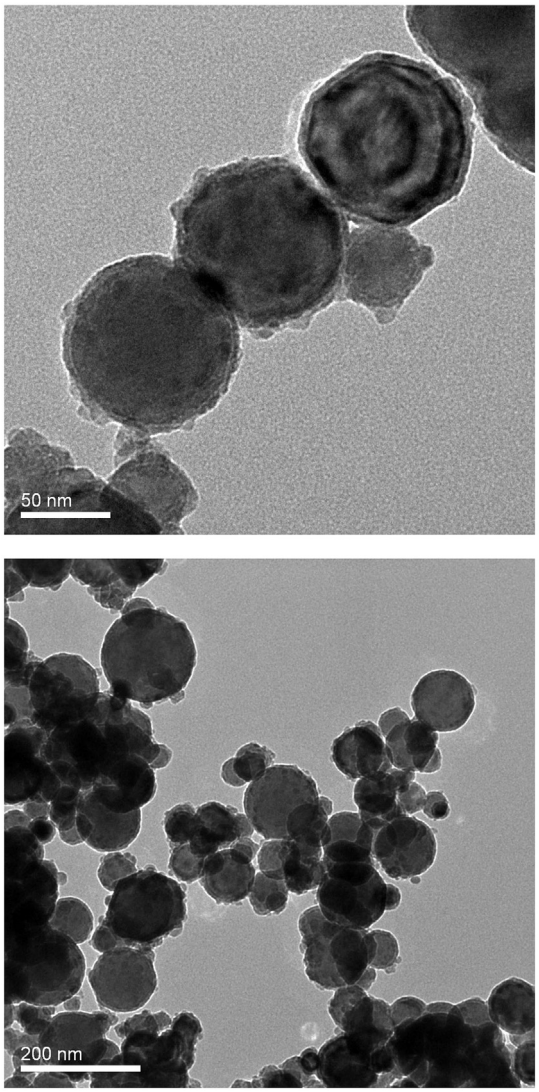

Fig. 1. The transmission electron microscopy (TEM) image of nZVI suspension.

2.2. Anoxic-oxic membrane bioreactor (A/O-MBR) setup

Three parallel laboratory-scale A/O-MBRs (Fig. S1) were operated with 0 mg/L (MBR-Blank), 25 mg/L (MBR-25 ppm) and 50 mg/L (MBR-50 ppm) nZVI discharged, respectively, for 80 days. For each A/O-MBR, a PVDF hollow fiber membrane module (total surface area = 260 cm^2; pore size = 0.4 μm; Litree Company, China) was equipped at the bottom of the oxic tank, and a constant fluid flux was set at 17 L/(m^2 h) with an intermittent suction mode (10 min/2 min on/off for each cycle). 0.4 m^3/h air was supplied continuously through a cross-flow action for effective scouring of membrane surface. The air flow rate was controlled with a gas flow-meter and trans-membrane pressure (TMP) was monitored with a pressure gauge. Hydraulic retention time (HRT) and solids retention time (SRT) were kept at 10 h and 30 days, respectively. The flow rate of recycled mixed liquor from the oxic tank to the anoxic tank was controlled at 200% of the influent flow rate (0.45 L/h).

The influent (with pretreatment, detailed in Supporting Information, SI) to the anoxic tank was the effluent from the aerated grit chamber, which was the first step of treatment in the Quyang municipal wastewater treatment plant (WWTP) (Shanghai, China). The influent pH and the reactor temperature remained within the range of 7.3–7.6 and 25–29 °C, respectively. The inoculating sludge was drawn from the return activated sludge stream in the Quyang WWTP, and washed with 0.9% NaCl solution for the original Fe removal (Fe in activated sludge was below 0.05 mg/g MLVSS (mixed liquor volatile suspended solids)). The newly inoculated A/O-MBR was initially operated for 60 days to achieve steady state for the acclimatization of activated sludge. The membrane module was then replaced with a new and similar unit and MBR was operated with an nZVI discharged (the final nZVI concentration was 0 mg/L in MBR-Blank, 25 mg/L in MBR-25 ppm and 50 mg/L in MBR-50 ppm) for 80 days. In addition, parallel A/O-MBRs with 0 mg/L, 25 mg/L and 50 mg/L nZVI discharged were also operated in the same condition for the reproducibility.

2.3. Extraction and measurement of extracellular polymeric substances (EPS)

Extraction of EPS from activated sludge was performed according to a modified thermal extraction method (Zhou et al., 2014a). 40 ml activated sludge was first centrifuged (MILTIFUGE X1R, Thermo Electron Corporation, USA) at 6000 g for 5 min and discharged the supernatant. The remaining sludge, re-suspended with 40 ml 0.9% NaCl solution, was shaken at 150 rpm for 10 min after 8 min ultrasound treatment (DS510DT, 40 kHz, 300 W, Shangchao, China). The mixed liquid was retreated with 4 min ultrasound and 30 min heating at 80 °C. The mixed liquid then was centrifuged at 12,000g for 20 min, and the supernatant was regarded as EPS. EPS has been normalized as the concentration of polysaccharide, protein, nucleic acid and humic acid (represented as TOC). They were measured by the phenol-sulfuric acid method, Branford method, diphenylamine method and TOC analyzer (TOC-V_{VPN}, Shimadzu, Japan), respectively (Xia et al., 2012).

2.4. Analysis of GC-MS

GC-MS (Focus DSQ, Thermo, USA) was carried out to identify the organic compounds of the membrane foulant. The sample was removed from the cake layer on the membrane surface and pretreated according to the description paper (Zhou et al., 2014c) (detailed in SI). Samples injection was done in the split mode (10:1)

into a VF-5 ms capillary column (30 m × 0.25 mm i. d. and 0.25 μm film thickness). Pure helium (99.999%) was used as GC carrier gas at a flow rate of 1.0 ml/min. The GC injector temperature was set at 200 °C. Oven temperature gradient started at 60 °C for 2 min and then increased (20 °C/min) to 300 °C for 10 min. The transfer line temperature was adjusted to 250 °C. Mass spectrometry conditions were as follows: electron ionization source set to 70 eV, MS source temperature set to 250 °C. The mass spectrometer was run in full-scan mode (m/z 41–450) and in selected-ion monitoring (SIM) mode according to the data of results. The results were employed to perform mass calculations and predictions according to National Institute of Standards and Technology (NIST).

2.5. ROS batch experiment

To determine the effect of nZVI ROS on activated sludge, ROS batch experiment were carried out according to Kim et al. (2009) with the activated sludge from MBR-Blank. *N*-Acetylcysteine (NAC) was reported as the antioxidant to reduce the ROS of nanoparticle (Kim et al., 2009; Mocan et al., 2010), and NAC was applied with different concentrations to protect bacteria from ROS shock due to nanoparticles. 25 mL activated sludge (3200 mg MLVSS/L) were added into 50 ml conical flask. The activated sludge was added with nZVI (0 mg/L and 50 mg/L, respectively) and NAC (0 mM, 1 mM, 2 mM, 5 mM and 10 mM, respectively). The activated sludge was cultured at 22 ± 1.0 °C for 24 h with 3.3 L/h air supply (similar air supply rate as MBR operation). Then the lactate dehydrogenase (LDH) in the supernatant of mixed liquid (LDH leakage, detailed in SI) was measured to determine the viability of activated sludge. The activated sludge remained at similar MLVSS during the experiment. Parallel batch experiments were performed for the reproducibility (n = 3).

2.6. Additional analysis

The determination of ammonia nitrogen (NH_4^+–N), total organic carbon (TOC), total nitrogen (TN), mixed liquor suspended solid (MLSS) and MLVSS were conducted in accordance with the Standard Methods (China-NEPA, 2002). The concentration of metal was analyzed via an inductively coupled plasma-optical emission spectrometer (ICP-OES, Optima 2100 DV, Perkin Elmer, USA) and atomic absorption spectroscopy (ASS, AA400, Perkin Elmer, USA) (detailed in SI). A focused beam reflectance measurement (EyeTech particle size and shape analyzer, Ankersmid, Holland) was used to analyze the particle size distribution (PSD) of the activated sludge. To determine the membrane foulant, a piece of membrane fiber was cut from the fouled (TMP = 40 kPa) membrane module. The membrane fiber with liquid N_2 pre-treatment was measured with scanning electron microscopy (SEM; XL30, Philips, Netherlands) coupled with an energy-dispersive X-ray analyzer (EDX; Oxford Isis, UK).

3. Results and discussion

3.1. Effects of loading nZVI discharged on reactor performance

Variations of the reactor performance between MBR-Blank, MBR-25 ppm and MBR-50 ppm were shown in Table 1. The decrease of pollutant (COD, NH_4^+–N and TN) removal efficiency indicated that nZVI discharged had negative effects on the pollutant bio-removal. At the initial 10 days after nZVI discharged, TN removal efficiency of MBR-25 ppm and MBR-50 ppm reached 70–75%, and pH was in the range of 7.7–7.9. At the initial 10 days, Fe^{n+} concentration increased from 11 ± 2.4 mg/L to 35 ± 3.1 mg/L in MBR-25 ppm and from 12 ± 1.2 mg/L to 40 ± 3.5 mg/L in MBR-50 ppm (Table S1). This was because nZVI worked as an electron donor for nitrate, promoting microbial removal of nitrate through below reactions (Eqs. (1)–(3) (Liu et al., 2014)).

$$4Fe^0 + NO_3^- + 7H_2O \rightarrow 4Fe^{2+} + NH_4^+ + 10OH^- \quad (1)$$

$$Fe^0 + 2H_2O \rightarrow Fe^{2+} + H_4^+ + 2OH^- \quad (2)$$

$$0.33NO_3^- + H_2 + 0.08CO_2 + 0.34H^+ \rightarrow 0.015C_5H_8O_2N + 0.16N_2 + 1.11H_2O \quad (3)$$

As Table S2 showed, MLVSS had an obvious decrease after the nZVI discharged, partly leading to the inhibition on the pollutant removal. Additionally, higher concentration of nucleic acid in EPS (Table S2) suggested that nZVI led to the bacterial cellular injury and cell death. nZVI could generate reactive oxygen species (ROS) under aerobic condition (Sevcu et al., 2012). Previous studies (Apel and Hirt, 2004; Cabiscol et al., 2010; Choi and Hu, 2008; Keenan and Sedlak, 2008) reported that ROS overload caused oxidative stress, protein damage and the inhibition neutralization, even killed bacteria. In addition, ROS was released into the cytosol and trigger ROS-induced ROS-release in other mitochondria (Keenan and Sedlak, 2008; Sevcu et al., 2012). In ROS batch experiment (Fig. S2), *N*-Acetylcysteine (antioxidant) effectively inhibited the ROS generation of nZVI. The LDH leakage increased obviously with nZVI addition, indicating that the bacterial cellular injury and cell death were due to the ROS generated by nZVI. Consequently, nZVI discharged led to the bacterial cellular injury and cell death, then inhibited the bacterial pollutant removal, due to the ROS generation.

3.2. Effects of loading nZVI discharged on activated sludge

Activated sludge plays a significant role in the membrane fouling process (Hao et al., 2016). As above mention, nZVI discharged caused the bacterial cellular injury and cell death, leading to biomass decrease. The particle size of activated sludge has a significant role on pore blocking and cake layer formation (Zhou et al., 2014b). The similar particle size distribution (Table 2) predicted that the nZVI discharged had no obvious effects on activated

Table 1
Average characteristics of the influent and effluent water (mg/L) of MBRs. (n = 60).

Parameters	MBR-Blank			MBR-25 ppm			MBR-50 ppm		
	Influent	Effluent	Removal (%)	Influent	Effluent	Removal (%)	Influent	Effluent	Removal (%)
COD	160 ± 84	8 ± 9	95 ± 1	158 ± 44	45 ± 6	71 ± 14	165 ± 60	53 ± 11	68 ± 18
NH_4^+–N	29 ± 5	1 ± 1	96 ± 1	28 ± 3	4 ± 2	85 ± 8	27 ± 4	6 ± 3	78 ± 12
TN	33 ± 5	11 ± 3	65 ± 2	31 ± 3	21±1[a]	32±3[a,b]	33 ± 5	22±1[a]	33±2[a,b]
TP	5 ± 1	2 ± 1	56 ± 6	6 ± 1	3 ± 1	57 ± 3	7 ± 3	3 ± 1	55 ± 3

[a] The effluent and removal data of TN was calculated after 10th day with nZVI discharged (n = 50).
[b] At the initial 10 days after nZVI discharged, TN removal efficiency of MBR-25 ppm and MBR-50 ppm reached 70 ± 7% and 74 ± 5%, respectively (n = 10).

Table 2
Particle size distributions of sludge flocs (n = 10).

Parameters	<1 μm	1–5 μm	5 10 μm	>10 μm	Mean size (μm)
MBR-Blank	0.0 ± 0.0%	3.1 ± 0.9%	58.5 ± 5.8%	38.4 ± 8.4%	9.84 ± 1.4
MBR-25 ppm	0.0 ± 0.0%	3.8 ± 0.7%	65.8 ± 7.8%	31.1 ± 6.4%	8.84 ± 0.9
MBR-50 ppm	0.1 ± 0.1%	4.0 ± 0.5%	62.2 ± 3.8%	33.8 ± 4.6%	8.77 ± 0.8

Table 3
Polysaccharides, protein and TOC of EPS in activated sludge after the long-tern operation of MBRs[a] (mg/g MLVSS) (n = 12).

	Polysaccharides	Protein	TOC
MBR-Blank	62 ± 8	18 ± 5	213 ± 12
MBR-25 ppm	38 ± 3	6.3 ± 3	75 ± 11
MBR-50 ppm	35 ± 4	5.8 ± 1	83 ± 7

[a] The data was calculated after the initial 10 days of nZVI discharged.

sludge particle size.

As the constructional material for activated sludge formation (Xia et al., 2012), EPS is a general and comprehensive concept for different classes of macromolecules, such as polysaccharides, proteins, humic acid and other polymeric compounds (Laspidou and Rittmann, 2002; Meng et al., 2009). At the initial 10 days after nZVI discharged, the increase of polysaccharides, protein and TOC in EPS (Table S3) was because of the cell lysis due to ROS generation of nZVI (Chaithawiwat et al., 2016; Lefevre et al., 2016). After the long-term operation of MBRs, the polysaccharides, protein and TOC of EPS had obvious decrease (Table 3), indicating that nZVI discharged inhibited the bacterial EPS release. Fajardo et al., (2013) reported that EPS (like protein) involved in the oxidative stress of nZVI. Additionally, the similar molecule weight (MW) distribution of EPS (Table 4) showed that the constitution of EPS had no obvious variation with the nZVI discharged. It was reported that the mitigation and inhibition functions of nZVI on bacterial activity was due to the nano-scale adsorption and oxidative stress (Chen et al., 2011; Lee et al., 2008). Therefore, nZVI discharged only inhibited the cell growth and the release of EPS from bacteria, but had no effects on the activated sludge particle size and the constitution of EPS.

3.3. Effects of nZVI discharged on membrane fouling

MBR-25 ppm and MBR-50 ppm kept a low TMP increase rate (approximately 42 Pa/h) for approximate 30 days, while MBR-Blank had a faster TMP increase rate from 21 to 166 Pa/h in 17 days (Fig. 2), indicating that nZVI discharged mitigated the membrane fouling process. Lots of crystals and cells were distributed on the membrane foulant surface in MBR-Blank (Fig. S3), but the membrane foulant surface in MBR-25 ppm and MBR-50 ppm only contained few of crystals and bacteria, indicating that nZVI discharged mitigated the accumulation of crystal and bacterial onto membrane surface. In addition, the membrane foulant thickness in MBR-25 ppm (17 μm) and MBR-50 ppm (13 μm) were approximately 3–4 times of that in MBR-Blank (48 μm), presenting the slight membrane fouling with nZVI discharged (Fig. 3).

Mg, Al, Si, Ca and Fe were the major inorganic elements in membrane foulant (Guo et al., 2012; Meng et al., 2009; Zhou et al., 2014b). nZVI discharged changed the distribution of inorganic elements in membrane foulant (Fig. 4; Fig. S4 showed the cross-sectional SEM image of new membrane surface). Element Si was reported in the form of SiO_2 in MBR (Zhou et al. 2014c, 2015). The rapid oxidation of nZVI increased Fe^{n+} (nZVI transformed into ferrous ions as Eq. (2); Fe^{n+} increased from 11 ± 2.4 mg/L to 19 ± 3.1 mg/L in MBR-25 ppm and from 12 ± 1.2 mg/L to 40 ± 3.5 mg/L in MBR-50 ppm) in the mixed liquor at the initial 10 days of nZVI discharged, leading to the particle precipitation (580 ± 50 mg Si/g precipitate in MBR-25 ppm and 650 ± 30 mg Si/g precipitate in MBR-50 ppm) by the Fe^{n+} flocculation and the decrease of Si percentage in the membrane foulant (Fig. 4). Additionally, the rapid oxidation of nZVI also released lots of OH^- (Eqs. (1)–(3)) and increased the pH of mixed liquor (average pH increased from 7.3 to 7.7) (Kumar et al., 2014; Liu et al., 2014). Most of Si was in the form of SiO_2 in membrane foulant, and accumulated onto membrane surface through the bidentate coordination with –COOH of the organic compounds (Fig. S5) (Zhou et al., 2014c). pH increase caused that the functional groups of organic compounds with Si were deprotonated and negatively charged, leading to the inhibition of organic compound accumulation on membrane surface (Lin et al., 2016; Schrittwieser et al., 2016). Additionally, SiO_2 had been reported as the major inorganic compounds causing membrane fouling. Consequently, nZVI obviously inhibited the accumulation onto membrane surface of organic compound with Si through pH increase, and further mitigated membrane fouling. The similar Fe cross-sectional distribution of membrane foulant in MBR-Blank, MBR-25 ppm and MBR-50 ppm (Fig. 3) indicated that nZVI discharged had no effects on the well distribution of Fe along the cross-section of membrane foulant.

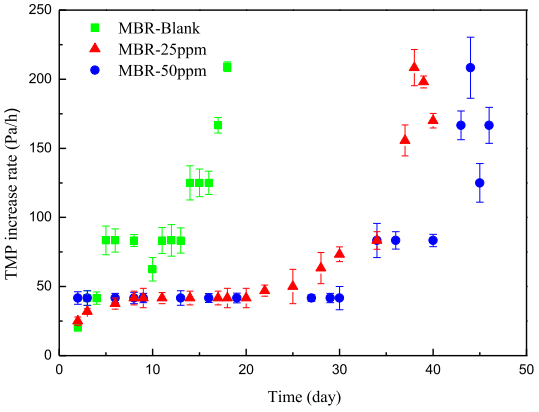

Fig. 2. Variations of TMP increase rate of MBRs (n = 6).

Table 4
Molecule weight distribution (%) of EPS in activated sludge of MBRs (n = 10).

MW(Da)	>10,000	10,000–5,000	5,000–1,000	1,000–500	500–100	<100
MBR-Blank	7.0 ± 1.4	3.7 ± 1.1	22.0 ± 4.3	42.9 ± 5.0	24.2 ± 4.1	0.0 ± 0.0
MBR-25 ppm	3.7 ± 0.9	3.0 ± 1.0	23.4 ± 2.4	46.8 ± 3.7	23.1 ± 2.5	0.0 ± 0.0
MBR-50 ppm	3.4 ± 0.7	2.3 ± 0.4	21.2 ± 2.0	50.8 ± 3.9	22.2 ± 3.5	0.1 ± 0.1

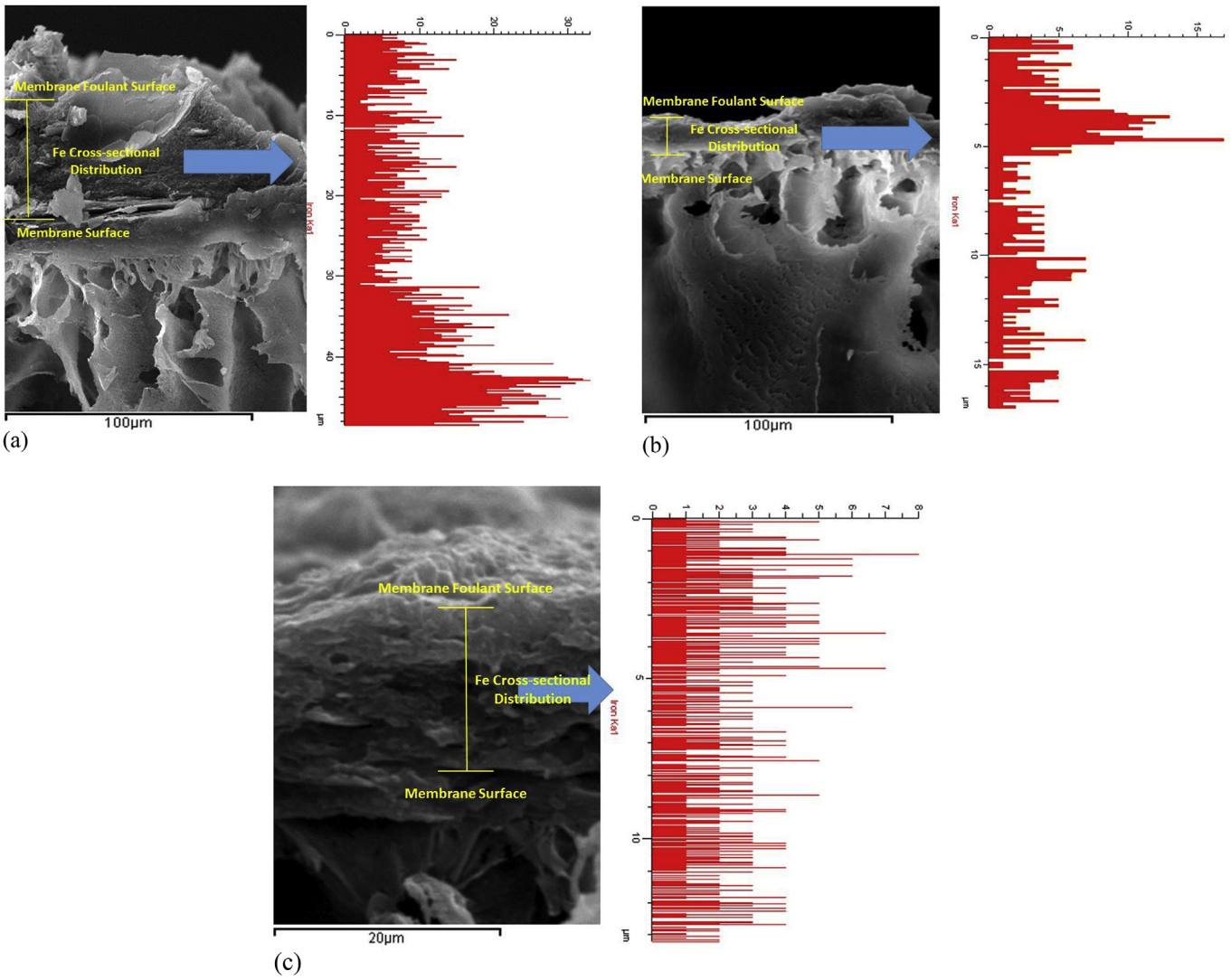

Fig. 3. The Fe cross-sectional distribution of membrane foulant in (a) MBR-Blank, (b) MBR-25 ppm and (c) MBR-50 ppm. (x-axis (μm) presented the thickness of cake layer, and unit was; y-axis (no unit) presented the intensity of Fe. Different magnification of each SEM images was due to various cake layer thickness.).

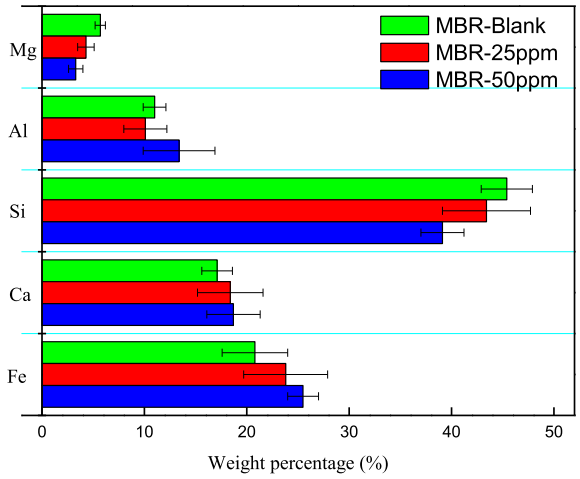

Fig. 4. Major inorganic element distribution of membrane foulant in MBRs with EDX analysis. (Two parallel membrane foulant samples for each MBRs was measured, and 3 different area of each sample were analyzed. n = 6).

The variations of VOCs in the membrane foulant were analyzed by GC-MS (Table 5). The VOCs of the membrane foulant can be classified into fatty acids (FA), *n*-alkanes (NA) and phthalate (PT), all of which are the major VOCs of activated sludge (Jarde et al., 2005). The nZVI discharged only induced the variations of each VOC proportion in membrane foulant. Although dibutyl phthalate became the majority VOC in membrane foulant, PT had the similar chemical characteristics as FA for membrane fouling (Zhou et al., 2014c), not leading to variations of membrane fouling.

As above results showed, the membrane fouling had been mitigated due to nZVI discharged. The similar activated sludge particle size, same EPS MW distribution and the resemblant constant VOCs constitution of membrane foulant indicated that the nZVI discharged would not affect membrane fouling through the above characteristics of activated sludge. In previous literature (Chang et al., 2014; Hong and He, 2014; Kim and Van der Bruggen, 2010), some membrane material modified with chemical oxidation nanoparticles (nano TiO_2, nano Ag, etc.) were applied to mitigate membrane fouling for providing the built-in oxidative functionality. In this study, nZVI generated ROS under aeration, leading to the cell lysis and bacteria death and further the decrease of biomass and EPS. The decreases of biomass and EPS promoted membrane

Table 5
The peak of the fragments of cake layer in MBRs by GC-MS

	Item		Retain time	Peak Area (%)		
				MBR-Blank	MBR-25 ppm	MBR-50 ppm
1	Phthalic acid, hept-4-yl isobutyl ester	FA	11.10	18.15	24.72	22.30
2	Hexadecanoic acid, methyl ester	FA	11.33	5.72	5.41	4.41
3	Dibutyl phthalate	PT	11.57	56.61	28.43	33.16
4	Heptadecanoic acid, 16-methyl-, methyl ester	FA	12.31	2.79	2.87	3.34
5	Heptacosane	NA	13.49	5.96	5.03	4.40
6	Phthalic acid, di (2-propylpentyl) ester	FA	14.15	10.77	33.54	32.39

FA: fatty acids; NA: n-alkanes; PT: phthalate.

fouling mitigation (Guo et al., 2012). Additionally, nZVI was also transformed into Fe^{n+}, which mitigates the fouling process of inorganic compounds (mainly Si element) through flocculation. Therefore, the mitigation of membrane fouling with missive nZVI discharged was also due to both oxidative stress to bacteria and Fe^{n+} flocculation of nZVI.

4. Conclusion

Loading nZVI discharged obviously mitigated the membrane fouling in a submerged A/O-MBR. nZVI transformed into Fe^{n+}, generated ROS and then caused oxidative stress, leading rapidly to the cell lysis and bacteria death, and further resulting in the decrease of biomass and EPS. nZVI also thinned the membrane fouling layer. But nZVI had no obvious effects on activated sludge particle size, EPS MW distribution and VOCs constitution of membrane foulant. Additionally, nZVI also released Fe^{n+} and mitigated the inorganic (mainly Si element) fouling by Fe^{n+} flocculation. Consequently, membrane fouling mitigation with nZVI discharged was mainly due to both oxidative stress to bacteria and Fe^{n+} flocculation of nZVI.

Acknowledgments

This work was supported by the National Natural Science Foundation of China (51378368) and the Foundation of State Key Laboratory of Pollution Control and Resource Reuse (Tongji University), China (PCRRT16003).

Appendix A. Supplementary data

Supplementary data related to this article can be found at http://dx.doi.org/10.1016/j.watres.2017.01.007.

References

Apel, K., Hirt, H., 2004. Reactive oxygen species: metabolism, oxidative stress, and signal transduction. Annu. Rev. Plant Biol. 55, 373–399.
Bagheri, S., Julkapli, N.M., 2016. Modified iron oxide nanomaterials: functionalization and application. J. Magn. Magn. Mater. 416, 117–133.
Cabiscol, E., Tamarit, J., Ros, J., 2010. Oxidative stress in bacteria and protein damage by reactive oxygen species. Int. Microbiol. 3 (1), 3–8.
Chaithawiwat, K., Vangnai, A., McEvoy, J.M., Pruess, B., Krajangpan, S., Khan, E., 2016. Role of oxidative stress in inactivation of Escherichia coli BW25113 by nanoscale zero-valent iron. Sci. Total Environ. 565, 857–862.
Chang, Q., Zhou, J.-e., Wang, Y., Liang, J., Zhang, X., Cerneaux, S., Wang, X., Zhu, Z., Dong, Y., 2014. Application of ceramic microfiltration membrane modified by nano-TiO< sub> 2 coating in separation of a stable oil-in-water emulsion. J. Membr. Sci. 456, 128–133.
Chen, J., Xiu, Z., Lowry, G.V., Alvarez, P.J., 2011. Effect of natural organic matter on toxicity and reactivity of nano-scale zero-valent iron. Water Res. 45 (5), 1995–2001.
China-NEPA, 2002. Water and Wastewater Monitoring Methods, fourth ed. Chinese Enviromental Science Publishing House, Beijing, China.
Choi, O., Hu, Z., 2008. Size dependent and reactive oxygen species related nanosilver toxicity to nitrifying bacteria. Environ. Sci. Technol. 42 (12), 4583–4588.
Davies, K.J.A., 2000. Oxidative stress, antioxidant defenses, and damage removal, repair, and replacement systems. Iubmb Life 50 (4–5), 279–289.
Fajardo, C., Saccà, M.L., Martinez-Gomariz, M., Costa, G., Nande, M., Martin, M., 2013. Transcriptional and proteomic stress responses of a soil bacterium Bacillus cereus to nanosized zero-valent iron (nZVI) particles. Chemosphere 93 (6), 1077–1083.
Feng, Y., Panwar, N., Tng, D.J.H., Tjin, S.C., Wang, K., Yong, K.T., 2016. The application of mesoporous silica nanoparticle family in cancer theranostics. Coord. Chem. Rev. 319, 86–109.
Guo, W., Ngo, H.-H., Li, J., 2012. A mini-review on membrane fouling. Bioresour. Technol. 122, 27–34.
Hao, L., Liss, S.N., Liao, B.Q., 2016. Influence of COD: N ratio on sludge properties and their role in membrane fouling of a submerged membrane bioreactor. Water Res. 89, 132–141.
Hong, J., He, Y., 2014. Polyvinylidene fluoride ultrafiltration membrane blended with nano-ZnO particle for photo-catalysis self-cleaning. Desalination 332 (1), 67–75.
Jarde, E., Mansuy, L., Faure, P., 2005. Organic markers in the lipidic fraction of sewage sludges. Water Res. 39 (7), 1215–1232.
Keenan, C.R., Sedlak, D.L., 2008. Factors affecting the yield of oxidants from the reaction of nanoparticulate zero-valent iron and oxygen. Environ. Sci. Technol. 42 (4), 1262–1267.
Kim, J., Van der Bruggen, B., 2010. The use of nanoparticles in polymeric and ceramic membrane structures: review of manufacturing procedures and performance improvement for water treatment. Environ. Pollut. 158 (7), 2335–2349.
Kim, S., Choi, J.E., Choi, J., Chung, K.-H., Park, K., Yi, J., Ryu, D.-Y., 2009. Oxidative stress-dependent toxicity of silver nanoparticles in human hepatoma cells. Toxicol. Vitro 23 (6), 1076–1084.
Kumar, N., Omoregie, E.O., Rose, J., Masion, A., Lloyd, J.R., Diels, L., Bastiaens, L., 2014. Inhibition of sulfate reducing bacteria in aquifer sediment by iron nanoparticles. Water Res. 51, 64–72.
Laspidou, C.S., Rittmann, B.E., 2002. A unified theory for extracellular polymeric substances, soluble microbial products, and active and inert biomass. Water Res. 36 (11), 2711–2720.
Lee, C., Kim, J.Y., Lee, W.I., Nelson, K.L., Yoon, J., Sedlak, D.L., 2008. Bactericidal effect of zero-valent iron nanoparticles on Escherichia coli. Environ. Sci. Technol. 42 (13), 4927–4933.
Lefevre, E., Bossa, N., Wiesner, M.R., Gunsch, C.K., 2016. A review of the environmental implications of in situ remediation by nanoscale zero valent iron (nZVI): behavior, transport and impacts on microbial communities. Sci. Total Environ. 565, 889–901.
Lin, X.X., Sun, X.Y., Luo, S.D., Liu, B., Yang, C.X., 2016. Development of DNA-based signal amplification and microfluidic technology for protein assay: a review. Trac-Trends Anal. Chem. 80, 132–148.
Liu, Y., Li, S., Chen, Z., Megharaj, M., Naidu, R., 2014. Influence of zero-valent iron nanoparticles on nitrate removal by Paracoccus sp. Chemosphere 108, 426–432.
Meng, F.G., Chae, S.R., Drews, A., Kraume, M., Shin, H.S., Yang, F.L., 2009. Recent advances in membrane bioreactors (MBRs): membrane fouling and membrane material. Water Res. 43 (6), 1489–1512.
Mocan, T., Clichici, S., Agoşton-Coldea, L., Mocan, L., Şimon, Ş., Ilie, I., Biriş, A., Mureşan, A., 2010. Implications of oxidative stress mechanisms in toxicity of nanoparticles (review). Acta Physiol. Hung. 97 (3), 247–255.
Navarro, E., Baun, A., Behra, R., Hartmann, N.B., Filser, J., Miao, A.J., Quigg, A., Santschi, P.H., Sigg, L., 2008. Environmental behavior and ecotoxicity of engineered nanoparticles to algae, plants, and fungi. Ecotoxicology 17 (5), 372–386.
Otero-Gonzalez, L., Garcia-Saucedo, C., Field, J.A., Sierra-Alvarez, R., 2013. Toxicity of TiO2, ZrO2, Fe-0, Fe2O3, and Mn2O3 nanoparticles to the yeast, Saccharomyces cerevisiae. Chemosphere 93 (6), 1201–1206.
Patil, S.S., Shedbalkar, U.U., Truskewycz, A., Chopade, B.A., Ball, A.S., 2016. Nanoparticles for environmental clean-up: a review of potential risks and emerging solutions. Environ. Technol. Innov. 5, 10–21.
Sacca, M.L., Fajardo, C., Martinez-Gomariz, M., Costa, G., Nande, M., Martin, M., 2014. Molecular stress responses to nano-sized zero-valent iron (nZVI) particles in the soil bacterium Pseudomonas stutzeri. PLoS One 9 (2).
Sacca, M.L., Fajardo, C., Nande, M., Martín, M., 2013. Effects of nano zero-valent iron on Klebsiella oxytoca and stress response. Microb. Ecol. 66 (4), 806–812.
Schrittwieser, S., Pelaz, B., Parak, W.J., Lentijo-Mozo, S., Soulantica, K., Dieckhoff, J.,

Ludwig, F., Guenther, A., Tschope, A., Schotter, J., 2016. Homogeneous biosensing based on magnetic particle labels. Sensors 16 (6).
Sevcu, A., El-Temsah, Y.S., Joner, E.J., Cernik, M., 2012. Oxidative stress induced in microorganisms by zero-valent iron nanoparticles. Microbes Environ. 27 (2), 215–215.
Xia, S., Zhou, L., Zhang, Z., Li, J., 2012. Influence and mechanism of N-(3-oxooxtanoyl)-L-homoserine lactone (C< sub> 8-oxo-HSL) on biofilm behaviors at early stage. J. Environ. Sci. 24 (12), 2035–2040.
Zhou, L., Xia, S., Alvarez-Cohen, L., 2015. Structure and distribution of inorganic components in the cake layer of a membrane bioreactor treating municipal wastewater. Bioresour. Technol. 196, 586–591.
Zhou, L., Zhang, Z., Jiang, W., Guo, W., Ngo, H.-H., Meng, X., Fan, J., Zhao, J., Xia, S., 2014a. Effects of low-concentration Cr (VI) on the performance and the membrane fouling of a submerged membrane bioreactor in the treatment of municipal wastewater. Biofouling 30 (1), 105–114.
Zhou, L., Zhang, Z., Meng, X., Fan, J., Xia, S., 2014b. New insight into the effects of Ca (II) on cake layer structure in submerged membrane bioreactors. Biofouling 30 (5), 571–578.
Zhou, L., Zhang, Z., Xia, S., Jiang, W., Ye, B., Xu, X., Gu, Z., Guo, W., Ngo, H.-H., Meng, X., 2014c. Effects of suspended titanium dioxide nanoparticles on cake layer formation in submerged membrane bioreactor. Bioresour. Technol. 152, 101–106.